RSC Advances

PAPER

View Article Online
View Journal | View Issue

Cite this: *RSC Adv.*, 2018, **8**, 32063

Removal of Pb(II) and Cr(VI) from aqueous solutions using the prepared porous adsorbent-supported Fe/Ni nanoparticles

Jiwei Liu,[ab] Min Dai,[c] Shaoxian Song[d] and Changsheng Peng *[ac]

In this study, Fe/Ni nanoparticles supported by a novel fly ash-based porous adsorbent (FBA-Fe/Ni) for Cr(VI) and Pb(II) removal were investigated. In order to enhance the reactivity of zero-valent iron (ZVI), ZVI particles were deposited on the surface or in the inner pores of FBA as a support material and Ni nanoparticles were introduced. FBA was prepared with the solid waste such as *Enteromorpha prolifera*, bentonite and fly ash. FBA-Fe/Ni was characterized *via* Fourier transform infrared spectroscopy, scanning electron microscopy, X-ray diffraction and the Brunauer–Emmett–Teller model and energy-dispersive spectrometry. The effects of various parameters on Cr(VI) and Pb(II) removal by FBA-Fe/Ni, such as FBA-Fe/Ni dosage, pH of the solution, reaction temperature, Cr(VI) and Pb(II) concentrations, co-existing ions and ionic strength were discussed. The possible removal mechanisms were proposed and the results indicated that there was a three-step reaction including the adsorption of Cr(VI) and Pb(II) on the surface of FBA-Fe/Ni, the subsequent reduction and precipitation. The removal capacity of Cr(VI) and Pb(II) by FBA-Fe/Ni was 25.07 mg g^{-1} and 164.19 mg g^{-1} at 303 K with an initial concentration of 1000 mg L^{-1} and FBA-Fe/Ni dosage of 0.20 g. In conclusion, this work demonstrated that FBA-Fe/Ni was a promising alternative material for Cr(VI) and Pb(II) removal.

Received 21st May 2018
Accepted 3rd August 2018

DOI: 10.1039/c8ra04324h

rsc.li/rsc-advances

Introduction

Environment contamination by heavy metals has become a serious problem for living organisms and public health in the last decade.[1] Lead and chromium are two major toxic metals, which are produced from mining, electronic equipment, leather tanning, metal processing and electroplating.[2] Due to non-biodegradability and high toxicity, lead and chromium ions pose a threat to human health and ecological systems. Therefore, it is urgently necessary to explore an effective, economical and environment-friendly treatment for lead and chromium removal.[3]

The treatment processes include adsorption, bio-mineralization and chemical precipitation for heavy metal removal.[4] Compared to the conventional methods, the adsorption is found to be an economic and effective method for removing heavy metals from wastewater due to its low-cost and effectivity in the removal process. Various adsorbent materials such as activated carbon, clay minerals, zeolites, agricultural waste, nanosized metal oxides and zero-valent iron are applied in heavy metals removal.[5] Among them, nZVI has drawn a great attention as one of the most effective adsorbents and reductants due to its strong reactivity and large surface area.[6] NZVI has a relatively low standard potential and can be oxidized to Fe^{2+} or Fe^{3+}. In this process, ZVI can provide electrons to heavy metals, converting them into the reduced forms.[7] Owing to the instability and aggregation of nZVI, there are still a lot of challenges with environmental application. In order to address this issue, the porous-based materials are used to support nZVI, such as chitosan, bentonite, kaolin and biochar, which can lead to a decrease in aggregation and oxidation of nZVI.[8] In addition, to further enhance the reactivity of nZVI, a second catalytic metal such as Pd or Ni was introduced.[9]

The aim of this research is to utilize the solid waste such as fly ash and *Enteromorpha prolifera* to prepare the porous adsorbent and support Fe/Ni nanoparticles. FBA as a support material was prepared with *Enteromorpha prolifera* as pore-forming agent, bentonite as binder and fly ash as skeletal material, which owned better chemical stability and larger surface area. Fe/Ni nanoparticles were synthesized by the chemical reduction method and loaded on FBA. The fly ash-based adsorbent-supported Fe/Ni nanoparticles was applied to remove Cr(VI) and Pb(II). Therefore, the studies include as follows: (i) the comparison of the removal capacity of lead using

[a]*The Key Lab of Marine Environmental Science and Ecology of Ministry of Education, Ocean University of China, Qingdao 266100, China. E-mail: pcs005@ouc.edu.cn*
[b]*School of Environment, Key Laboratory for Solid Waste Management and Environment Safety, Ministry of Education of China, Collaborative Innovation Center for Regional Environmental Quality, Tsinghua University, Beijing, 100084, China*
[c]*School of Environmental and Chemical Engineering, Zhaoqing University, Zhaoqing, 526061, China*
[d]*School of Resources and Environmental Engineering, Wuhan University of Technology, Wuhan, 430070, China*

FBA, FBA-ZVI and FBA-Fe/Ni; (ii) the characterization of FBA-Fe/Ni before and after removal experiments; (iii) the influence of different factors on the removal of Cr(VI) and Pb(II); (iv) the analysis of removal mechanisms of Cr(VI) and Pb(II) removal.

Experimental

Chemicals and materials

All chemicals were of analytical reagent grade and used without further pretreatment. Sodium borohydride ($NaBH_4$), lead nitrate ($Pb(NO_3)_2$), ferric chloride hexahydrate ($FeCl_3 \cdot 6H_2O$), potassium dichromate ($K_2Cr_2O_7$), nickel sulfate hexahydrate ($NiSO_4 \cdot 6H_2O$) and other agents were purchased from Tianjin Chemical Reagent Co. (Tianjin, China).

Bentonite was obtained from Qingdao city, China. Fly ash was purchased from Rizhao city, China. *Enteromorpha prolifera* was collected from Qingdao city, China.

Preparation of FBA and FBA-Fe/Ni

Fly ash, *Enteromorpha prolifera* and bentonite were dried and sieved through a 200-mesh screen. According to a fly ash/bentonite/*Enteromorpha prolifera* mass ratio of 6 : 3 : 1, three kinds of materials with deionized water were blended for 30 min. The mixed materials were mechanically formed to rod-like particles and rod-like particles were dried at 105 °C for 12 h. Rod-like particles were sintered at 600 °C with a 10 °C min^{-1} heating rate for 60 min in atmosphere sintering furnace. A novel fly ash-based porous adsorbent was obtained.

FBA-Fe/Ni was prepared by conventional liquid-phase reduction method and FBA was used as a support material.[10] The procedure was as follows: (1) 4.52 g $FeCl_3 \cdot 6H_2O$ with/without 0.28 g $NiSO_4 \cdot 6H_2O$ was added to the mixture of water and ethanol (10 mL distilled water + 40 mL absolute ethanol) and dissolved in a capped conical flask. 3.00 g FBA were added to the mixtures and they were shaken at room temperature and 150 rpm for 12 h. FBA was taken out from solution and rinsed several times with absolute ethanol; (2) 2.14 g $NaBH_4$ and 0.20 g NaOH were dissolved in 50 mL of deionized water and the prepared FBA was added into the solution under a nitrogen atmosphere. They were shaken at room temperature and 150 rpm for 12 h; (3) the prepared FBA-Fe/Ni were taken out from the solution, rinsed several times with absolute ethanol and dried in a vacuum oven at 65 °C for 24 h. Schematic diagram of the preparation of FBA-Fe/Ni is observed in Fig. 1.

Materials characterization

The crystalline phases of FBA and FBA-Fe/Ni were determined by X-ray diffraction (XRD, D/max-γB). The scanning electron microscope (SEM/EDX, JSM-6700F) was used to characterize the surface morphology. The elemental mapping of FBA-Fe/Ni surface was captured to determine the distribution of elements (SEM/EDX, JSM-6700F). The energy dispersive X-ray spectroscopy (SEM/EDX, JSM-6700F) was applied to analyze the elemental information of FBA and FBA-Fe/Ni. The specific surface areas of FBA and FBA-Fe/Ni were assessed by BET method (Micromeritics' ASAP 2020). FTIR spectra of samples were recorded between 400 and 4000 cm^{-1} at room temperature (FTIR, Bruker Vertex 70).

Removal experiment

To evaluate the Pb(II) removal potential of various adsorbents, a batch removal experiment was carried out using FBA(0.20 g), FBA-ZVI (0.20 g) and FBA-Fe/Ni (0.20 g) added into 100 mL solution of Pb(II) concentration of 1000 mg L^{-1} in the conical flask at 303 K and 120 rpm for 24 h.

The effects of different factors such as FBA-Fe/Ni dosage (0.20–1.20 g), Pb(II) and Cr(VI) concentration (200–1000 mg L^{-1}), pH (1–11), contact time (0–24 h), reaction temperature (293–313 K), cations (K^+, Na^+, Mg^{2+}, Ca^{2+}), anions (NO_3^-, Cl^-, PO_4^{3-}, SO_4^{2-}) and ionic strength (0.01–0.1 mol L^{-1}) on Cr(VI) and Pb(II) removal were investigated.

Fig. 1 Schematic diagram of FBA-Fe/Ni preparation.

Regeneration experiment of FBA-Fe/Ni was carried out as follows. To start, 0.20 g of FBA-Fe/Ni was added to 100 mL of 1000 mg L^{-1} Cr(VI) and Pb(II) solutions in the flasks and shaken at 313 K and 120 rpm for 24 h, and separated from the solutions. Afterward, FBA-Fe/Ni separated from Pb(II) solution was added to 0.10 mol L^{-1} HCl solution and FBA-Fe/Ni separated from Cr(VI) solution was added to 0.10 mol L^{-1} NaOH solution. The mixtures were shaken at 313 K and 120 rpm for 12 h and rinsed several times with deionized water until the pH value of the solution was approximately 7. Thirdly, Fe/Ni nanoparticles were supported on FBA-Fe/Ni by the liquid-phase reduction method once again.[11] Subsequently, the regenerated FBA-Fe/Ni was employed again for Cr(VI) and Pb(II) removal. These procedures were repeated for four recycles.

The residual concentration Cr(VI) was measured by the 1,5-diphenylcarbazide method at a wavelength of 540 nm using a UV-VIS spectrophotometer. The residual concentration of Pb(II) was measured using a atomic absorption spectrophotometer. The removal capacity of Cr(VI) and Pb(II) at was calculated as follows:

$$q_t = \frac{(C_0 - C_t) \times V}{w} \quad (1)$$

Here, q_t (mg g^{-1}) represents the removal capacity, V is the volume of the solution, w (g) represents the weight of FBA-Fe/Ni, C_0 and C_t (mg L^{-1}) are the concentration of Cr(VI) and Pb(II) in the aqueous solutions at initial and time t, respectively.

Results and discussion

Characterizations

The morphology of FBA-Fe/Ni is presented in Fig. 2(a and b). A lot of different size pores distributed in FBA. That was because that *Enteromorpha prolifera* at different sizes as a pore former were burnt out or decomposed during heating process, leaving a lot of pores in FBA material.[12] The pore size was controlled by pore-forming agent types, sizes and additive amount. In addition, the sintering temperature and time determined the surface area of FBA.[13] In addition, it was figured out clearly that the Fe/Ni nanoparticles were chain-like or spherical in shape with a diameter in the range of several nanometers to several microns and deposited in the inner pores and on the surface of FBA-Fe/Ni, which were slightly agglomerated because of its magnetism. EDS revealed that Fe, Ni, C and O were present in FBA-Fe/Ni. The contents of Ni (2 wt%) and Fe (14 wt%) in FBA-Fe/Ni were measured, proving that Fe/Ni was successfully deposited in FBA. The content of Fe^0 in FBA-Fe/Ni was measured to be 18.22 mg g^{-1} by ferric chloride leaching–potassium dichromate titration method. Furthermore, elemental mapping images of Fe and Ni further indicated the presence of Fe and Ni in FBA-Fe/Ni (Fig. 2(c and d)).

The XRD patterns of FBA and FBA-Fe/Ni are revealed in Fig. 2(e). It showed that there was an apparent peak at 44.69° in Fig. 2(e), which confirmed the existence of Fe^0 in FBA-Fe/Ni compared to the pattern of FBA.[14] It could be concluded that Fe^0 were successfully loaded on the surface or in the inner pores of FBA and existed in FBA-Fe/Ni. However, the characteristic peak of Ni^0 was weak and not observed due to a low Ni^0 loading. These results were consistent with the SEM, EDS and elemental mapping analysis.

The FTIR analysis of FBA, FBA-Fe/Ni, FBA-Fe/Ni/Pb and FBA-Fe/Ni/Cr was performed using FTIR spectra meter as shown in Fig. 2(f). The characteristic peak at 3400 cm^{-1} was assigned to the –OH in the FTIR spectra of FBA, which was strong adsorption site. Compared to the FTIR spectra of FBA, the characteristic peak at 3400 cm^{-1} in the FTIR spectra of FBA-Fe/Ni became stronger after the synthesis of Fe/Ni nanoparticles, indicating the formation of FeOOH layer on the surface of nZVI. The peaks at 1620 cm^{-1} and 1420 cm^{-1} corresponded to the –COOH, confirming the existence of carboxyl group. For FBA-Fe/Ni/Pb and FBA-Fe/Ni/Cr, a new peak was observed at 570 cm^{-1}, which belonged to the Fe–O bending vibration. This indicated the corrosion of Fe nanoparticles as a reductant to form oxide of Fe(II) and Fe(III) after reaction. The intensities of peaks at 1620 cm^{-1}, 1420 cm^{-1} and 3400 cm^{-1} had changed after Pb(II) and Cr(VI) removal. This was because of the chelating of Pb(II) and Cr(VI) with these functional groups.[15]

To investigate the textural properties, N_2 adsorption–desorption isotherm and pore size distribution were determined as illustrated in Fig. 2(g and h). Based on the obtained data, the specific surface areas of FBA and FBA-Fe/Ni were 36.32 m^2 g^{-1} and 20.63 m^2 g^{-1} and the average pore size of FBA and FBA-Fe/Ni was 3.04 nm and 2.89 nm, respectively. Compared to the specific surface area of FBA, the specific surface area of FBA-Fe/Ni decreased, which was caused by the fact that Fe nanoparticles were embedded into the inner pores of FBA and occupied the pore volume. According to IUPAC classifications, N_2 adsorption–desorption isotherm was classified as type (IV) with H1 hysteresis loop, which reflected the presence of mesoporous structure in FBA and FBA-Fe/Ni. According to pore size distribution curves, its showed a broad peak in the range (2–10) nm, which indicated that FBA-Fe/Ni showed well-developed mesopores distribution of FBA and FBA-Fe/Ni.[16] This also demonstrated that the pore diameters and volumes of FBA-Fe/Ni became smaller.

Removal of Pb(II) using FBA, FBA-ZVI and FBA-Fe/Ni

To evaluate the performance of FBA, FBA-ZVI and FBA-Fe/Ni, the removal of Pb(II) by various materials were investigated as shown in Fig. 3. The removal capacity of Pb(II) by FBA-ZVI was higher than that by FBA, indicating that nZVI was successfully synthesized and deposited on the surface or in the inner pores of FBA. In addition, the removal capacity and rate of Cr(VI) and Pb(II) by FBA-Fe/Ni were higher than that by FBA-ZVI, suggesting that the introduction of Ni as a catalyst enhanced catalytic reduction and adsorption ability for Pb(II).[17] Hence, it was concluded that FBA played an important role as a support material and Ni could enhance the reactivity of ZVI as a catalyst, which made FBA-Fe/Ni become a potential material for Pb(II) removal.

Effects of initial concentration

The influence of Cr(VI) and Pb(II) concentration on removal capacity were tested as presented in Fig. 4. The removal

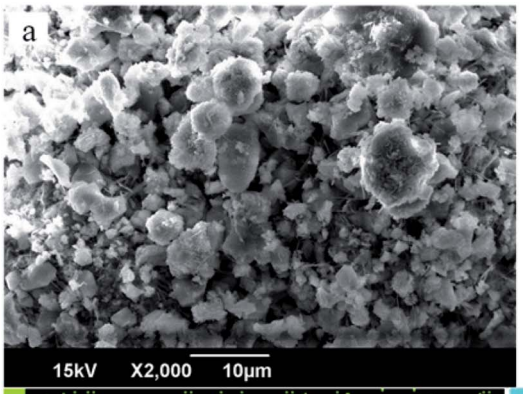

b EDS

Element	Mass (%)
C	14.99
O	45.62
Na	10.65
Al	1.56
Si	4.04
S	2.15
Cl	0.72
Ca	6.89
Fe	11.38
Ni	2

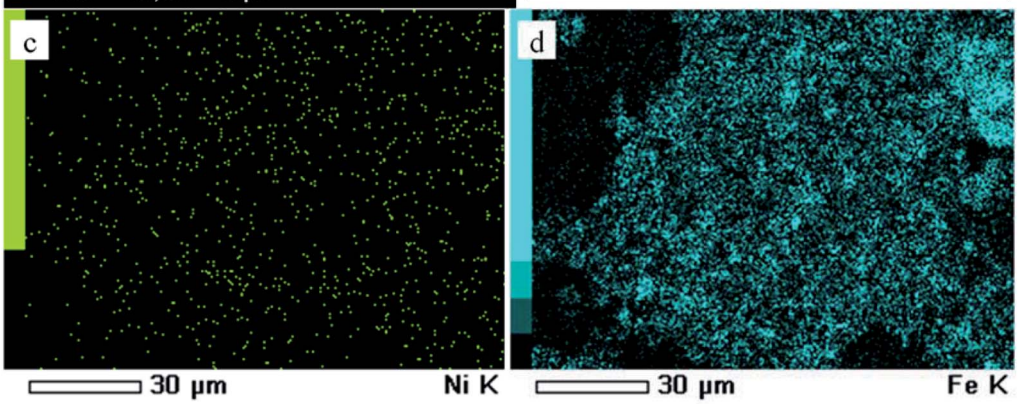

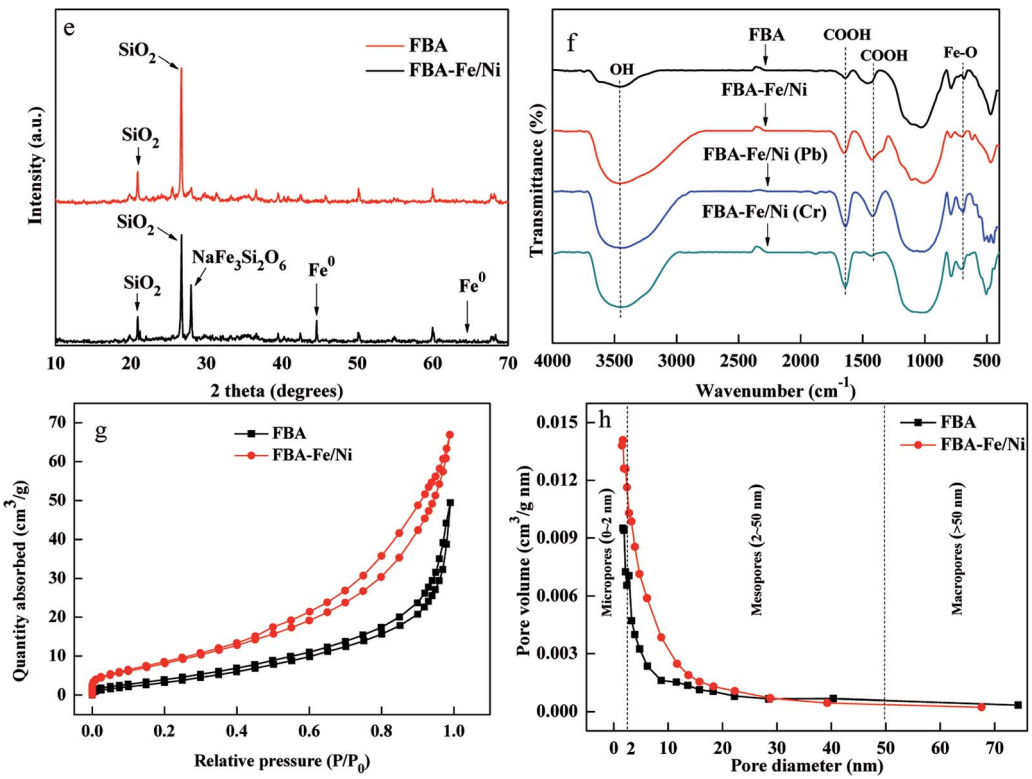

Fig. 2 (a and b) SEM/EDS images of FBA-Fe/Ni; (c and d) elemental mapping images of Fe and Ni in FBA-Fe/Ni; (e) XRD patterns of FBA and FBA-Fe/Ni; (f) FTIR spectra of FBA and FBA-Fe/Ni before and after the reaction; (g) N_2 adsorption–desorption isotherms; (h) pore size distributions of FBA and FBA-Fe/Ni.

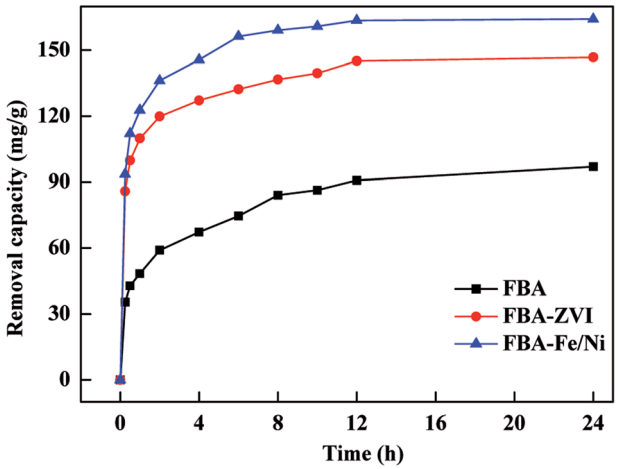

Fig. 3 The removal capacity of Pb(II) using FBA, FBA-ZVI and FBA-Fe/Ni.

capacity of Cr(VI) and Pb(II) increased with an increase in contact time from 0 h to 24 h. The removal capacity and rate of Cr(VI) and Pb(II) were higher due to larger surface area, more active sites and more content of Fe^0 in the initial phase, which indicated that there was a high affinity and reducing power between FBA-Fe/Ni, Cr(VI) and Pb(II). The removal capacity of Cr(VI) and Pb(II) by FBA-Fe/NI increased as the concentration of Cr(VI) and Pb(II) increased. This was due to the fact that the probability of the collision between Cr(VI), Pb(II) and active sites on the surface of FBA-Fe/Ni improved. Furthermore, the high concentration of Cr(VI) and Pb(II) could provide the driving force to overcome mass transfer resistances between the solid phases and aqueous solution. However, the increased removal capacity of Cr(VI) and Pb(II) was low when the concentration of Cr(VI) and Pb(II) increased from 200 mg L^{-1} to 1000 mg L^{-1}. This phenomenon was attributed to the fact that a passivated lead (chromium) layer formed quickly on the surface of nZVI and occupied the active sites at higher concentration of Cr(VI) and Pb(II), which would reduced the electron transfer and inhibited the adsorption and reduction of Cr(VI) and Pb(II).[18]

Effect of FBA-Fe/Ni dosage

The influence of FBA-Fe/Ni dosage on the removal of Cr(VI) and Pb(II) was determined as shown in Fig. 5. The removal efficiency of Cr(VI) and Pb(II) increased with an increase in FBA-Fe/Ni dosage from 0.20 to 1.20 g while the removal capacity of Cr(VI) and Pb(II) decreased as FBA-Fe/Ni dosage increased. The increase in the removal efficiency was attributed to an increase in the availability of Fe^0 content, active sites and specific surface area in FBA-Fe/Ni. In addition, the removal capacity of Cr(VI) and Pb(II) decreased due to the fact that the relative surface area, active sites and Fe^0 content in FBA-Fe/Ni decreased as FBA-Fe/Ni dosage increased.[19]

Effect of initial pH

The influence of pH value of the solution on Cr(VI) and Pb(II) removal was evaluated as presented in Fig. 6. The functional groups, surface charge of FBA-Fe/Ni and the form of Cr(VI) and Pb(II) affect the overall removal process. The pH can change the form of Cr(VI) and Pb(II) existing in aqueous solution, surface charge of FBA-Fe/Ni and the ionization state of functional groups. Pb ions exist in the aqueous solution as Pb(II) below pH 6.0 while Cr ions exist in the aqueous solution as $HCrO_4^-$ between pH 1.0 and 6.0 and CrO_4^{2-} above pH 6.0.[20] There were various kinds of functional groups such as hydroxyl and carboxyl groups on the surface of FBA-Fe/Ni. As shown in Fig. 6, the removal capacity of Pb(II) increased as an increase in pH from 1.0 to 6.0 while the removal capacity Cr(VI) decreased as an increase in pH from 1.0 to 11. The behavior could be explained by the fact that functional groups such as carboxyl and hydroxyl groups were easily protonated and become positively charged at low pH, which was favorable for the adsorption of negatively charged $HCrO_4^-$ onto the surface of FBA-Fe/Ni. In addition, the reduction of Cr(VI) to Cr(III) by Fe^0 was highly dependent on the pH of the solution because H^+ could promote the corrosion of Fe^0 and improve electron transfer from FBA-Fe/Ni to Cr(VI), which led to an increase in the reduction of Cr(VI) to Cr(III) by Fe^0.[21] However, the competition of reactive sites between Pb(II) and H^+ would restrain the adsorption of Pb(II) and improve the reduction of Pb(II) to Pb^0 at lower pH. Positively charged Pb(II)

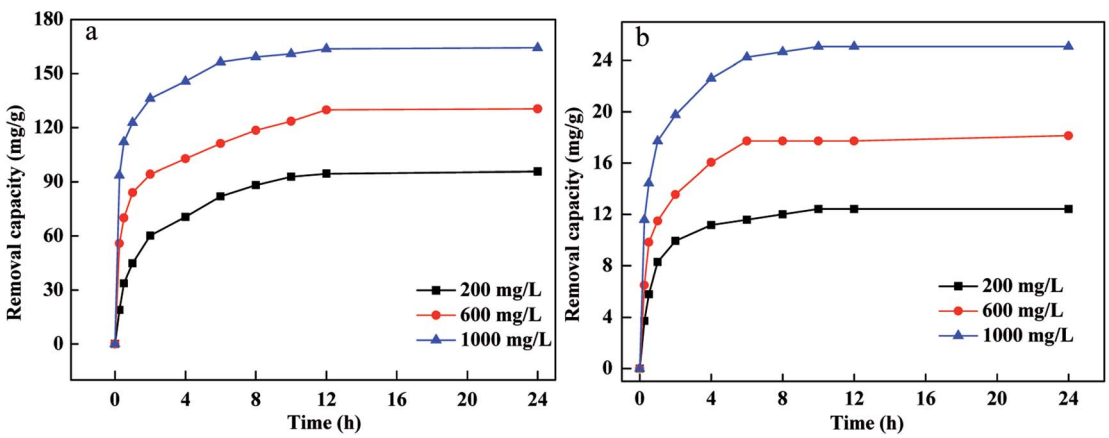

Fig. 4 Effects of contact time and initial concentration on the removal of Pb(II) (a) and Cr(VI) (b)by FBA-Fe/Ni.

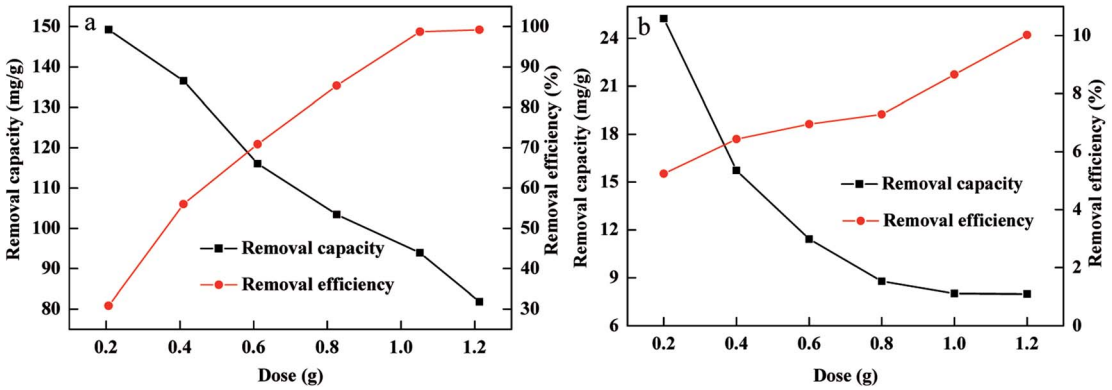

Fig. 5 Effect of FBA-Fe/Ni dosage on the removal of Pb(II) (a) and Cr(VI) (b) by FBA-Fe/Ni.

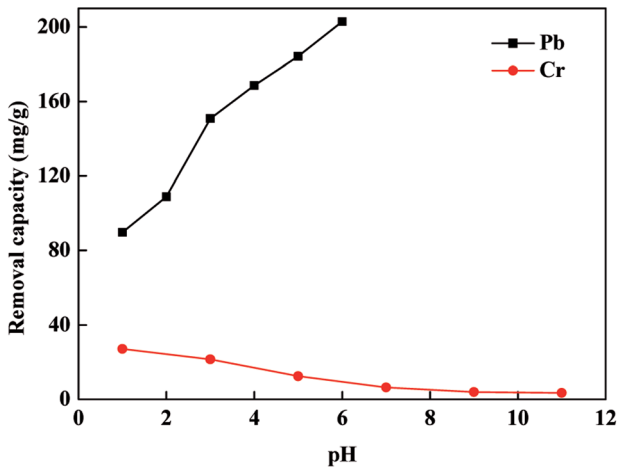

Fig. 6 Effect of pH on the removal of Pb(II) and Cr(VI) by FBA-Fe/Ni.

was favorably adsorbed onto the negatively charged surface of FBA-Fe/Ni at higher pH. Moreover, with the increase in the solution pH, the enhancement in the amount of OH^- resulted in the formation of iron hydroxide layer on the surface of FBA-Fe/Ni, which prevented the electrons transport from Fe^0 to Cr(VI) and Pb(II).[22]

Effect of reaction temperature

The influence of reaction temperature on Cr(VI) and Pb(II) removal was evaluated as shown in Fig. 7. It was clear that the removal rate increased when the reaction temperature rose from 293 K to 313 K, implying that the removal process was endothermic in nature. The reason for this was that the transfer rate of Cr(VI) and Pb(II) ions increased from the solution to the surface of FBA-Fe/Ni and the diffusion rate of Cr(VI) and Pb(II) ions in the inner pores was accelerated under the higher temperature. The removal capacity increased as an increase in the temperature. This was because that the pores largened and the surface area improved as an increase in the temperature.[23] In addition, when the reaction temperature increased, the radiuses of hydrated Cr(VI) and Pb(II) decreased, making more Cr(VI) and Pb(II) diffuse into the small pores. Moreover, Cr(VI) and Pb(II) reacted more effectively with the active sites on surface of FBA-Fe/Ni at higher temperature.[24]

Effect of co-existing ions and ionic strength

The effects of cations (Na^+, K^+, Ca^{2+}, Mg^{2+}) on of Pb(II) removal and anions (Cl^-, NO_3^-, SO_4^{2-}, PO_4^{3-}) on Cr(VI) removal were discussed as presented in Fig. 8(a and c). The results demonstrated that the presence of Na^+ and K^+ had not obviously

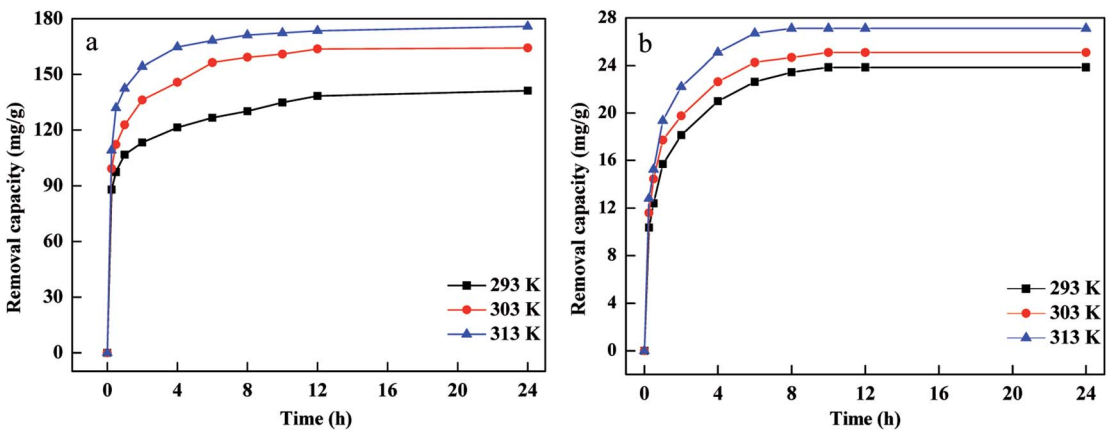

Fig. 7 Effect of temperature on the removal of Pb(II) (a) and Cr(VI) (b) by FBA-Fe/Ni.

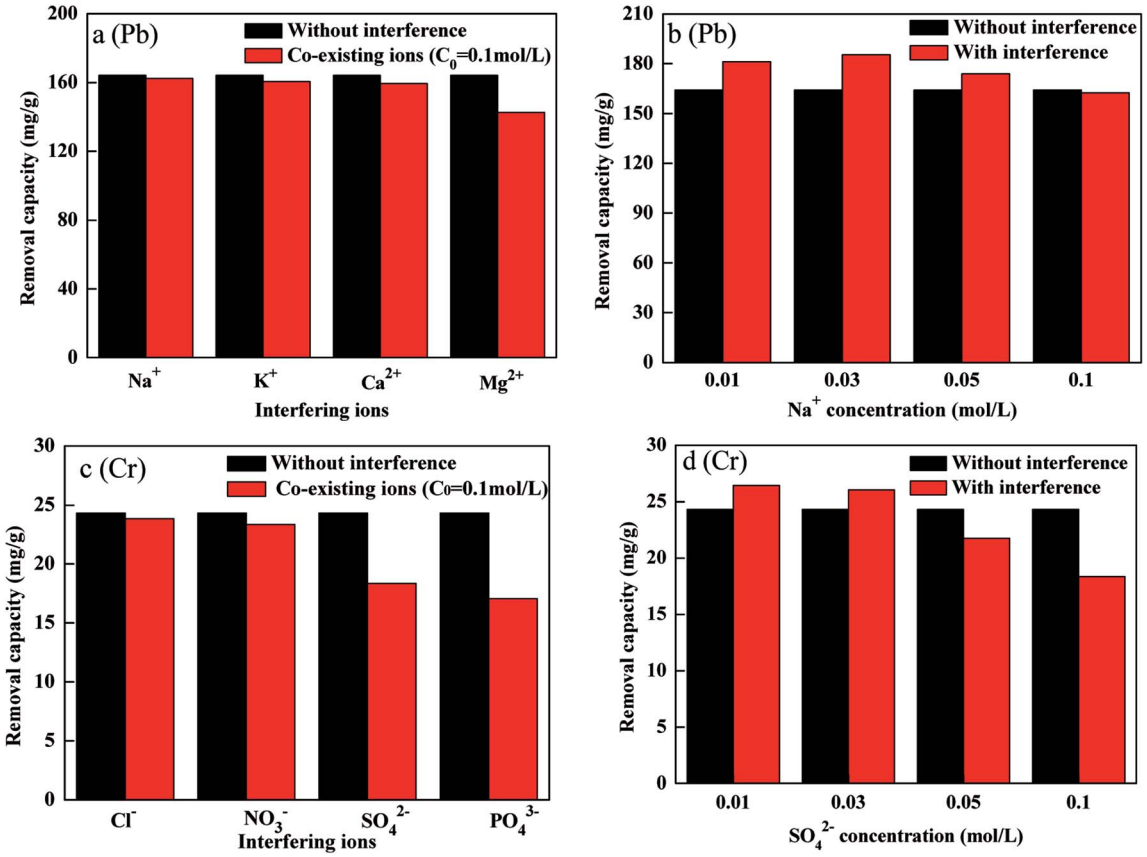

Fig. 8 Effect of co-existing ions and ionic strength on the removal of Pb(II) (a and b) and Cr(VI) (c and d) by FBA-Fe/Ni.

impact on Pb(II) removal. In the addition, the removal of Pb(II) slightly decreased in the presence of Ca^{2+} and Mg^{2+}.[25] The phenomenon was ascribed to the competitive adsorption of Ca^{2+}, Mg^{2+} and Pb(II) at the active sites. The presence of Cl^- and NO_3^- slightly decreased Cr(VI) removal while SO_4^{2-} and PO_4^{3-} obviously decreased Cr(VI) removal. The competitive adsorption of SO_4^{2-}, PO_4^{3-} and Cr(VI) ions at the active sites led to a decrease in the removal of Cr(VI).[26] The removal of Cr(VI) and Pb(II) by FBA-Fe/Ni was not only an adsorption process, but also a reduction and co-precipitation process. As shown in Fig. 8(b and d), Na^+ and SO_4^{2-} at lower concentration could promote the removal of Cr(VI) and Pb(II). The reason for this was that the corrosion of Fe^0 enhanced due to the presence of interfering ions and increased ionic strength could accelerate the diffusion of the precipitate of lead (chromium)/iron oxide away from the surface of FBA-Fe/Ni.[27,28]

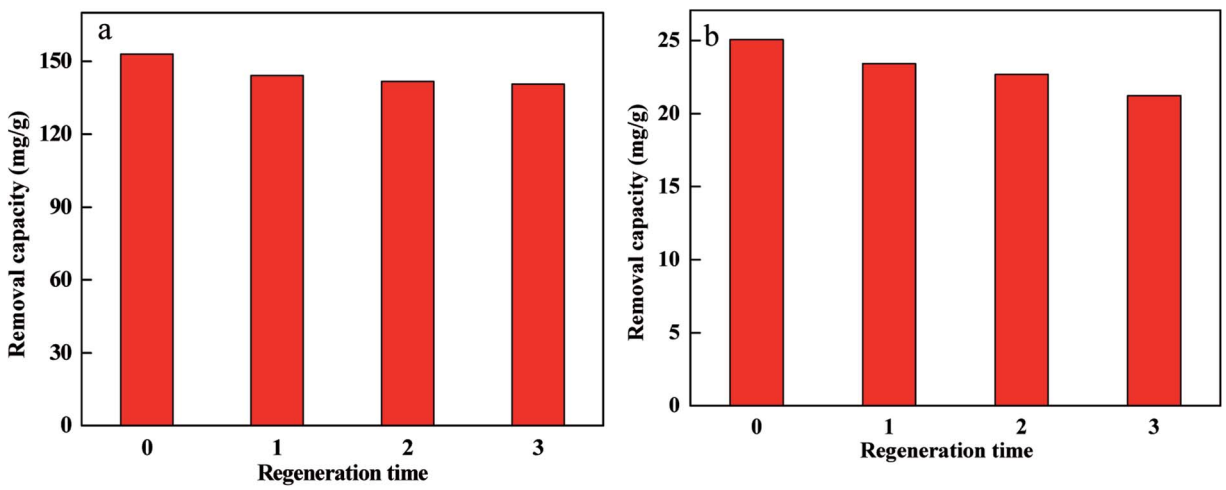

Fig. 9 Reusability of FBA-Fe/Ni for Pb(II) (a) and Cr(VI) (b) removal.

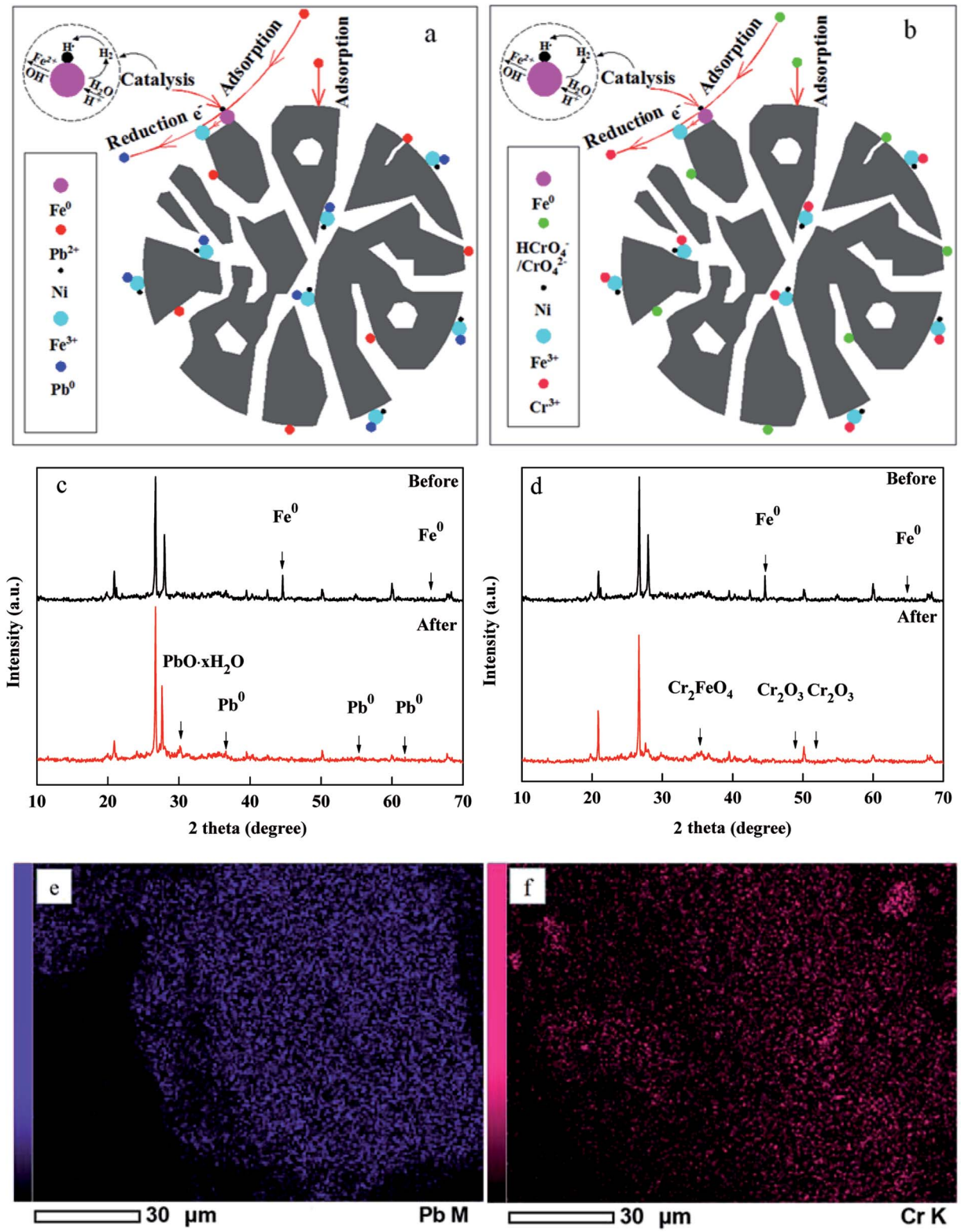

Fig. 10 (a and b) Mechanisms of the interaction of Pb(II) and Cr(VI) with FBA-Fe/Ni; (c and d) XRD patterns of FBA-Fe/Ni before and after the reaction with Pb(II) and Cr(VI); (e and f) Element mapping images of FBA-Fe/Ni after the reaction with Pb(II) and Cr(VI).

Reuse of FBA-Fe/Ni

Repeated use of FBA-Fe/Ni is an important parameter for the adsorbent to assess the cost of wastewater treatment[28] as presented in Fig. 9. The results indicated that the removal capacity of Cr(VI) and Pb(II) by FBA-Fe/Ni slightly decreased. This was because that a small amount of Cr(VI) and Pb(II) was still on

Table 1 Comparison of the removal capacity of Pb(II) and Cr(VI) by various adsorbents

Adsorbent	Metal	q_m (mg g^{-1})	Reference
FBA-Fe/Ni	Pb(II)	164.19	This study
Kaolin-supported NZVI	Pb(II)	90.00	7
3D hierarchical flower-like nickel ferrite/manganese dioxide	Pb(II)	85.78	37
Multifunctional nanocomposites Fe_3O_4@SiO_2–EDTA	Pb(II)	114.94	38
Carbon gel-supported Fe-graphene disks	Pb(II)	170.00	39
FBA-Fe/Ni	Cr(VI)	25.07	This study
CTAB modified magnetic nanoparticles	Cr(VI)	10.05	40
Ficus carica biosorbent	Cr(VI)	19.68	41
Magnetic magnetite (Fe_3O_4) nanoparticle	Cr(VI)	34.87	42
Biochar-supported nanoscale zero-valent iron	Cr(VI)	40.00	43

the surface or in the inner pores of FBA-Fe/Ni and occupied the active sites, resulting in a slight decrease in the removal capacity, which proved that FBA-Fe/Ni was low-cost and potential adsorbent for Cr(VI) and Pb(II) removal.

Removal mechanisms

According to previous literatures, the removal of Cr(VI) and Pb(II) by FBA-Fe/Ni was an adsorption, reduction and co-precipitation process as follows: (i) Pb(II), CrO_4^{2-} and $HCrO_4^-$ ions in aqueous solution diffused from the solution to the surface of FBA-Fe/Ni; (ii) Pb(II), $HCrO_4^-$ and CrO_4^{2-} ions diffused from the external surface to the inner pores; (iii) Pb(II), $HCrO_4^-$ and CrO_4^{2-} ions were adsorbed onto the surface of FBA-Fe/Ni and simultaneously reduced and precipitated (Fig. 10(a and b)).[29,30] In this process, due to the introduction of Ni^0, galvanic celled formed between Fe^0 and Ni^0, leading to a continuous electron flow and the enhancement in the activity of Fe^0. The corrosion of Fe^0 provided the electrons to Ni^0 and Cr(VI), Pb(II) ions accepted the electrons, which were reduced to Cr(III) and Pb^0.[31,32]

In order to better understand the mechanisms of Cr(VI) and Pb(II) by FBA-Fe/Ni and confirm the species of Cr and Pb on the surface of FBA-Fe/Ni, the XRD patterns of FBA-Fe/Ni before and after removal experiments were analyzed and the results are shown in Fig. 10(c and d). As shown in Fig. 10(c and d), an apparent peak of Fe^0 before removal experiments was observed and weakened obviously after the reaction with Pb(II) and Cr(VI). In addition, the XRD patterns indicated the presence of Pb^0, $Pb{\cdot}xH_2O$, Cr_2O_3 and Cr_2FeO_4 after the reaction with Cr(VI) and Pb(II). This demonstrated the redox reaction between Cr(VI), Pb(II) and Fe^0. Cr(VI) and Pb(II) ions were reduced to Cr(III) and Pb^0 by Fe^0 under the catalysis of Ni^0.[33,34] Afterwards, the corrosion of Fe^0 released Fe(II) and OH^-. The precipitation and co-precipitation of Pb(II) hydroxides, Cr(III) hydroxides and Fe/Cr (oxy)hydroxides occurred in the inner pores or on the surface of FBA-Fe/Ni.[35]

To further confirm the presence of Pb and Cr element in FBA-Fe/Ni, the element mapping analysis of FBA-Fe/Ni after the reaction with Pb(II) and Cr(VI) was performed as shown in Fig. 10(e and f). It was obviously observed that Cr and Pb element existed in FBA-Fe/Ni.[36]

Comparison of various adsorbents

The removal capacity of FBA-Fe/Ni with various adsorbents for Cr(VI) and Pb(II) reported in literature was compared and the results are listed in Table 1. The results indicated that FBA-Fe/Ni possessed higher Cr(VI) and Pb(II) removal capacity. In addition, FBA-Fe/Ni was potentially applied to remove toxic heavy metals.

Conclusion

A new fly ash-based porous adsorbent-supported Fe/Ni nanoparticles (FBA-Fe/Ni) was prepared and used to remove Cr(VI) and Pb(II) from aqueous solutions. SEM analysis indicated that Fe/Ni nanoparticles were successfully deposited in the inner pores or on the surface of FBA. EDX and XRD analysis indicated the presence of Fe/Ni nanoparticles. FTIR analysis indicated FBA-Fe/Ni had different functional groups responsible for the adsorption of heavy metals. BET indicated that FBA-Fe/Ni was a porous adsorbent. The removal capacity of Cr(VI) and Pb(II) increased with reaction temperature and Cr(VI) and Pb(II) concentrations. In addition, the removal capacity of Cr(VI) and Pb(II) decreased with the increase of the dosage of FBA-Fe/Ni. Moreover, the removal capacity of Cr(VI) decreased with the increase of the solution pH while the removal capacity of Pb(II) increased with the increase of the solution pH. The presence of anions (NO_3^-, Cl^-, PO_4^{3-}, SO_4^{2-}) and cations (K^+, Na^+, Mg^{2+}, Ca^{2+}) had impact on Cr(VI) and Pb(II) removal. The reuse experiment of FBA-Fe/Ni proved that FBA-Fe/Ni could be well reused under the appropriate regeneration conditions. The possible removal mechanism included the adsorption of Cr(VI) and Pb(II), the subsequent reduction of Cr(VI) to Cr(III) and Pb(II) to Pb^0 and the precipitation of Pb(II) hydroxides, Cr(III) hydroxides and Fe(III)/Cr(III) hydroxides. Therefore, the application of FBA-Fe/Ni demonstrated that FBA-Fe/Ni presented an excellent performance on heavy metal remediation.

Conflicts of interest

There are no conflicts to declare.

Acknowledgements

The authors acknowledge the support of the State Key Laboratory of Environmental Criteria and Risk Assessment (SKLECRA2013FP12) and the Shandong Province Key Research and Development Program (2016GSF115040).

References

1 M. A. Behnajady and S. Bimeghdar, *Chem. Eng. J.*, 2014, **239**, 105–113.
2 T. Wang, Y. Gao, X. Jin and Z. Chen, *Chin. J. Environ. Eng.*, 2013, **7**, 3476–3482.
3 N. Arancibia-Miranda, S. E. Baltazar, A. García, D. Munoz-Lira, P. Sepúlveda, M. A. Rubio and D. Altbir, *J. Hazard. Mater.*, 2016, **301**, 371–380.
4 A. R. Esfahani, A. F. Firouzi, G. Sayyad, A. Kiasat, L. Alidokht and A. R. Khataee, *Res. Chem. Intermed.*, 2014, **40**, 431–445.
5 M. Anbia and N. Mohammadi, *J. Porous Mater.*, 2011, **18**, 13–21.
6 R. A. Crane, M. Dickinson and T. B. Scott, *Chem. Eng. J.*, 2015, **262**, 319–325.
7 X. Zhang, S. Lin, X. Q. Lu and Z. L. Chen, *Chem. Eng. J.*, 2010, **163**, 243–248.
8 H. Su, Z. Fang, P. E. Tsang, L. Zheng, W. Cheng, J. Fang and D. Zhao, *J. Hazard. Mater.*, 2016, **318**, 533–540.
9 X. Liu, Z. Chen, Z. Chen, M. Megharaj and R. Naidu, *Chem. Eng. J.*, 2013, **223**, 764–771.
10 H. Li, Y. F. Qiu, X. L. Wang, J. Yang, Y. J. Yu, Y. Q. Chen and Y. D. Liu, *Chemosphere*, 2017, **169**, 534–541.
11 A. S. Özcan, Ö. Gök and A. Özcan, *J. Hazard. Mater.*, 2009, **161**, 499–509.
12 J. Zhang, B. Jiang and D. Wang, *Algal Res.*, 2016, **18**, 45–50.
13 Y. Yin, J. Fang and Q. Xue, *Int. J. Refract. Met. Hard Mater.*, 2017, **67**, 82–89.
14 X. Zhang, S. Lin, Z. Chen, M. Megharaj and R. Naidu, *Water Res.*, 2011, **45**, 3481–3488.
15 H. Shirzadi and A. Nezamzadeh-Ejhieh, *J. Mol. Liq.*, 2017, **230**, 221–229.
16 A. Soliemanzadeh and M. Fekri, *Microporous Mesoporous Mater.*, 2017, **239**, 60–69.
17 X. Weng, Q. Sun, S. Lin, Z. Chen, M. Megharaj and R. Naidu, *Chemosphere*, 2014, **103**, 80–85.
18 S. A. Drweesh, N. A. Fathy, M. A. Wahba, A. A. Hanna, A. I. M. Akarish, E. A. M. Elzahany, I. Y. El-Sherif and K. S. Abou-El-Sherbini, *J. Environ. Chem. Eng.*, 2016, **4**, 1674–1684.
19 P. Li, K. Lin, Z. Fang and K. Wang, *J. Cleaner Prod.*, 2017, **151**, 21–33.
20 L. N. Shi, X. Zhang and Z. L. Chen, *Water Res.*, 2011, **45**, 886–892.
21 H. Dong, J. Deng, Y. Xie, Z. Cong, J. Zhao, Y. Cheng, K. Hou and G. Zeng, *J. Hazard. Mater.*, 2017, **332**, 79–86.
22 H. Asiabi, Y. Yamini and M. Shamsayei, *J. Hazard. Mater.*, 2017, **339**, 239–247.
23 M. H. Fatehi, J. Shayegan, M. Zabihi and I. Goodarznia, *J. Environ. Chem. Eng.*, 2017, **5**, 1754–1762.
24 M. Arshadi, M. Soleymanzadeh, J. W. Salvacion and F. Salimivahid, *J. Colloid Interface Sci.*, 2014, **426**, 241–251.
25 Z. Xin, L. Shen, X. Q. Lu and Z. Chen, *Chem. Eng. J.*, 2010, **163**, 243–248.
26 R. Fu, Y. Yang, X. Zhen, X. Zhang, X. Guo and D. Bi, *Chemosphere*, 2015, **138**, 726–734.
27 M. Soleymanzadeh, M. Arshadi, J. W. L. Salvacion and F. Salimivahid, *Chem. Eng. Res. Des.*, 2015, **93**, 696–709.
28 X. Lv, Y. Hu, J. Tang, T. Sheng, G. Jiang and X. Xu, *Chem. Eng. J.*, 2013, **218**, 55–64.
29 W. Wang, Y. Hua, S. Li, W. Yan and W. X. Zhang, *Chem. Eng. J.*, 2016, **304**, 79–88.
30 L. Liang, Q. Chen, F. Jiang, D. Yuan, J. Qian, G. Lv, H. Xue, L. Liu, H. Jiang and M. Hong, *J. Mater. Chem. A*, 2016, **4**, 15370–15374.
31 X. Zhou, G. Jing, B. Lv, Z. Zhou and R. Zhu, *Chemosphere*, 2016, **160**, 332–341.
32 J. Qian, P. Yua and S. Huang, *CrystEngComm*, 2016, **18**, 7955–7958.
33 Y. Xi, M. Mallavarapu and R. Naidu, *Mater. Res. Bull.*, 2010, **45**, 1361–1367.
34 G. Quan, J. Zhang, J. Guo and Y. Lan, *Water, Air, Soil Pollut.*, 2014, **225**, 1979.
35 T. Liu, X. Yang, Z. Wang and X. Yan, *Water Res.*, 2013, **47**, 6691–6700.
36 Y. Zhang, Y. Li, J. Li, G. Sheng, Y. Zhang and X. Zheng, *Chem. Eng. J.*, –.
37 X. Bo, L. Dong, L. Han and H. Gu, *J. Hazard. Mater.*, 2016, **325**, 178–188.
38 Y. Liu, R. Fu, Y. Sun, X. Zhou, S. A. Baig and X. Xu, *Appl. Surf. Sci.*, 2016, **369**, 267–276.
39 S. Mishra, A. Yadav and N. Verma, *Chem. Eng. J.*
40 S. A. Elfeky, S. E. Mahmoud and A. F. Youssef, *J. Adv. Res.*, 2017, **8**, 435–443.
41 V. K. Gupta, D. Pathania, S. Agarwal and S. Sharma, *Environ. Sci. Pollut. Res. Int.*, 2013, **20**, 2632–2644.
42 S. Rajput, P. C. Jr and D. Mohan, *J. Colloid Interface Sci.*, 2016, **468**, 334–346.
43 L. Qian, W. Zhang, J. Yan, L. Han, Y. Chen, D. Ouyang and M. Chen, *Environ. Pollut.*, 2017, **223**, 153–160.

